International Journal of Bioprinting

RESEARCH ARTICLE

Three-dimensional printing of microfiber-reinforced hydrogel loaded with oxymatrine for treating spinal cord injury

Shiqiang Song[1†], Jing Zhou[2†], Junming Wan[3†], Xingchang Zhao[1†], Kai Li[4], Chengliang Yang[1], Chuanchuan Zheng[1], Liqiang Wang[5], Yujin Tang[1*], Chong Wang[6*], Jia Liu[1*]

[1]Guangxi Key Laboratory of Basic and Translational Research of Bone and Joint Degenerative Diseases, Guangxi Biomedical Materials Engineering Research Center for Bone and Joint Degenerative Diseases, Department of Orthopedics, Affiliated Hospital of Youjiang Medical University for Nationalities, Baise, Guangxi, 533000, China

[2]Youjiang Medical University for Nationalities, Baise, Guangxi, 533000, China

[3]Department of Orthopaedics Surgery, The Seventh Affiliated Hospital, Sun Yet-sun University, Shenzhen, Guangdong, 518000, China

[4]The Third Affiliated Hospital of Southern Medical University, Guangzhou, Guangdong, 510663, China

[5]State Key Laboratory of Metal Matrix Composites, School of Material Science and Engineering, Shanghai Jiao Tong University, Shanghai, 200240, China

[6]School of Mechanical Engineering, Dongguan University of Technology, Dongguan, Guangdong, 523808, China

[†]These authors contributed equally to this work.

***Corresponding authors:**
Yujin Tang
(tangyujin1967@163.com)

Chong Wang
(wangchong@dgut.edu.cn)

Jia Liu
(liujia0111@live.cn)

Citation: Song S, Zhou J, Wan J, *et al*., 2023, Three-dimensional printing of microfiber-reinforced hydrogel loaded with oxymatrine for treating spinal cord injury. *Int J Bioprint*, 9(3): 692.
https://doi.org/10.18063/ijb.692

Received: September 22, 2022
Accepted: December 16, 2022
Published Online: February 22, 2023

Abstract

Spinal cord injury (SCI) causes severe neural tissue damage and motor/sensory dysfunction. Since the injured spinal cord tissue has limited self-regeneration ability, several strategies, including cell therapy, drug delivery, and tissue engineering scaffold implantation, have been employed to treat SCI. However, each of these strategies fails to obtain desirable outcomes due to their respective limitations. In comparison, advanced tissue engineering scaffolds with appropriate topographical features, favorable composition, and sustained drug delivery capability can be employed to recruit endogenous neural stem cells (NSCs), induce neuronal differentiation, and facilitate neuron maturation. This can lead to the regeneration of injured spinal cord tissue and the recovery of motor function. In this study, fiber bundle-reinforced spinal cord extracellular matrix hydrogel scaffolds loaded with oxymatrine (OMT) were produced through near-field direct write electrospinning. The spinal cord extracellular matrix-based hydrogel was then coated with OMT. The physical/chemical properties and *in vitro* degradation behavior of the composite scaffolds were investigated. The *in vitro* cell culture results showed that composite scaffolds loaded with OMT promoted the differentiation of NSCs into neurons and inhibited differentiation into astrocytes. The *in vivo* results showed that the composite scaffolds loaded with OMT recruited NSCs from the host tissue, promoted neuronal differentiation and axon extension at the lesion site, inhibited glial scar formation at/around the lesion site, and improved the recovery of motor function in rats with SCI. To sum up, 3D-printed microfiber-reinforced spinal cord extracellular matrix hydrogel scaffolds loaded with OMT are promising biomaterials for the treatment of SCI.

Keywords: Spinal cord injury; 3D bioprinting; Spinal cord extracellular matrix; Oxymatrine; Glial scar; Nerve regeneration

1. Introduction

Spinal cord injury (SCI) can result in serious damage to the central nervous system. It is caused mainly by trauma and has an annual global incidence of about 10.4–83 cases per million[1,2]. SCI can cause motor, sensory, and autonomic dysfunction below the level of the injury[3,4]. The pathological process of SCI is complex but can be divided into two stages: a primary injury that leads to neuronal and axonal rupture, necrosis, and demyelination; a secondary injury that consists of various pathophysiological mechanisms, including local hemorrhage, ischemia, edema, ion imbalance, free radical stress, and inflammatory responses. Ultimately, local inhibitory protein expression increases local scarring and cystic cavity formation, and this local inhibitory microenvironment is detrimental to neural tissue regeneration[5-9]. Although partial recovery can be achieved in patients with SCI, their recovery and quality of life would still be undesirable due to the high incidence of complications, such as urinary tract infections and pressure ulcers[10,11]. Current strategies to treat SCI include traditional drug therapy, cell therapy, gene therapy, and tissue engineering scaffold implantation. These strategies cannot fully repair SCI, but are only able to alleviate symptoms and reduce complications[12]. Therefore, it is imperative to explore effective therapeutic strategies.

Three-dimensional (3D) printing for making advanced tissue engineering scaffolds is an emerging technology. Its advantage is that it endows scaffolds with a customized shape, biomimetic structure, and tailored porosity. Through this technology, many tissues and organs have been made[13,14]. Meanwhile, biomolecules and even living cells can be encapsulated within 3D-printed scaffolds to obtain enhanced functionality. The selection of biomaterials is crucial for the therapeutic effect, and a desirable bioscaffold should be based on excellent biocompatibility, mechanical strength, biodegradability, and bioactivity. Polycaprolactone (PCL) is a biodegradable polymer with good mechanical properties that can provide physical support for spinal cord regeneration. However, the biological activity of PCL is relatively poor. The hydrogel has good biological activity but poor mechanical strength, so the combination of the two can satisfy the requirements of the scaffold in mechanical strength and biological activity.

In recent years, decellularized extracellular matrix (ECM) has been widely used as the material matrix or additive to fabricate tissue engineering scaffolds with improved composition and similarity. They have been used to repair/regenerate bone[15,16], cartilage[17,18], muscle[19], skin[20], heart[21-23], blood vessels[24], bladder[25], kidney[26], vocal cords[27], nerves[28], uterus[29], and esophagus[30,31]. The ECM of the central nervous system constitutes a complex 3D network that participates in the regulation of cellular functions in the central nervous system and promotes axonal regeneration after injury[32]. In our previous study, decellularized spinal cord scaffolds were implanted in rats with a spinal cord hemisection with the goal of promoting axon regeneration and motor function recovery[33]. Considering that the spinal cord ECM hydrogel retains the original extracellular components, it can act as a desirable microenvironment to induce favorable cellular responses.

Oxymatrine (OMT) is a quinazoline alkaloid isolated from the root of *Sophora flavescens*. It has anti-inflammatory, anti-fibrotic, and anti-tumor activities. It is used to treat viral hepatitis, cancer, viral myocarditis, gastrointestinal bleeding, and skin diseases[34,35]. Researchers have confirmed that OMT plays an important role in the protection and repair of spinal cord injury because it can greatly restore motor function by reducing oxidative stress, inflammatory responses, and apoptosis[36,37]. In addition, the anti-fibrotic effects of OMT suggest that it has the potential to prevent local scar formation after SCI.

In this study, we fabricated microfiber-reinforced spinal cord ECM hydrogel-based scaffolds loaded with OMT by 3D printing technology. The biocompatibility, degradability, cumulative release of OMT, and mechanical property of the composite scaffolds were verified *in vitro*.

The composite scaffolds were implanted into a semi-transected part of the spinal cord in rats to study its repair effects on SCI and to find a new method for treating SCI. Our study found that the composite scaffold could guide the directional growth of axons, reduce scarring, and promote the recovery of motor function in rats.

2. Materials and methods

2.1. Fabrication of the bracket

2.1.1. Spinal cord decellularized scaffold

Healthy adult Sprague-Dawley (SD) rats (purchased from Changsha Tianqin Biotechnology Co., Ltd.) were anesthetized with 3% sodium pentobarbital by intraperitoneal injection. Each rat was fixed on the operating table in the prone position, and about 3 cm of the thoracic spinal cord was removed for future use. The spinal cord tissues were frozen at −80°C for 1 h and then thawed at room temperature. They were soaked in double-distilled water for 6 h, with water changes every hour. The spinal cord tissues were then placed in 1% TritonX-100 phosphate buffer and shaken at room temperature for 3 h (25°C, 100 rpm). They were then further shaken and rinsed with double-distilled water for 3 h with water changes every hour. They were placed in 1% sodium deoxycholate buffer

and shaken continuously for 3 h at room temperature. They were shaken and rinsed with double-distilled water for 3 h with water changes every hour. The above steps were repeated once. The extracted spinal cord was placed in sterile phosphate buffer saline (PBS, 0.01 mol/L, pH 7.2) and stored in a refrigerator at 4°C for later use. After setting the freeze-dryer program, the spinal cord decellularized scaffold was freeze-dried for 24 h, after which it was stored for later use.

2.1.2. Spinal cord ECM hydrogel

The rat acellular spinal cord (ASC) scaffold was ground and digested into a matrix solution using liquid nitrogen and then mixed with polymer materials, such as water, gelatin, β-cyclodextrin, polyethylene glycol diacrylate, and a photoinitiator. The mixed material was divided into two parts. One part was kept as the original polymer solution, and the other was loaded with OMT to prepare a spinal cord ECM drug-loaded hybrid polymer solution. The spinal cord ECM hydrogel was then irradiated with 300–410 nm ultraviolet light for 5–15 min.

2.1.3. Polycaprolactone microfiber

The organic polymer PCL was dissolved in the organic solvent trifluoroethanol to form a polymer solution. The polymer solution was transferred to an electrospinning machine to prepare PCL microfibers with the same orientation.

The abovementioned spinal cord ECM hydrogels and OMT-loaded supramolecular hydrogels were **uniformly** coated on PCL microfibers, which were then **slowly** curled **lengthwise** into a cylindrical-like structure (similar to the spinal cord morphology), **about half the diameter of the adult rat spinal cord** and subjected to UV light irradiation. The 3D-printed spinal cord ECM hydrogel microfiber scaffolds loaded with OMT were obtained by crosslinking. The prepared composite scaffolds were packaged, sterilized with cobalt-60 gamma rays (3K GY), and stored at a low temperature for future use (Figure 1).

2.2. Scanning electron microscopy

A scanning electron microscope (SEM) (Zeiss, Germany) was used to observe the scaffold surface and cross-sectional morphology. The prestored composite scaffold was taken out, and its surface was sprayed with gold, observed, and photographed with a SEM at a voltage of 3 kV.

2.3. Scaffold degradation test

The degradation rate of the scaffolds was tested by weighing them under dry conditions (Wo) and placing them in a PBS solution at room temperature. The PBS solution was replaced every 3 days. The scaffolds were removed at 2, 4, 6, and 8 weeks, frozen, and then freeze-dried. Their weight (Wt), degradation rate, and ratio to the original weight were determined.

$$\text{Degradation rate} = (Wt - Wo)/Wo \times 100\%$$

2.4. Cumulative release of OMT

The *in vitro* sustained release behavior of OMT was determined by dialysis. The samples were placed in a dialysis bag (MWCO: 1000), then 50 mL PBS (pH 7.4) solution was added and oscillated on a shaker set at 75 r/min and a constant temperature of 37°C. At the set time node, 2 mL of the released solution was removed and the same volume of fresh PBS was added. The concentration of OMT in the medium was determined by high-performance liquid chromatography (HPLC).

2.5. Testing the mechanical properties of the scaffold

Tensile and compression tests were carried out on each group of scaffold samples at 37°C, and the strain rate was set at 2 mm/min. The same test was repeated three times.

2.6. *In vitro* co-culture

2.6.1. Seeding of neural stem cells

The scaffolds were placed in 96-well plates, and the second-generation neural stem cells (NSCs) were seeded with a pipette on the sterile scaffolds at a density of 1×10^6 cells/mL. A control group was set.

2.6.2. In vitro viability assay of NSCs

Cell viability was assessed using a calcein-AM/propidium iodide (PI) cell double-staining kit. NSCs (1×10^5 NSCs) were resuspended in centrifuge tubes and seeded in 96-well plates. After 12 h, the medium was changed to a proliferation medium. NSCs were seeded in 96-well plates loaded with scaffold (control group) and scaffold + OMT (treated group). They were then double-stained with calcein-AM and PI at 37°C for 15 min. Observation and photography were carried out with a laser confocal microscope.

2.6.3. Immunofluorescence staining

Cells were fixed with 4% paraformaldehyde fixative, rinsed three times with PBS at room temperature, and blocked with 10% goat serum blocking solution at room temperature for 1 h. Cells were incubated with primary antibodies (TUJ1, MAP2, GFAP, dilution ratio: 1:200) overnight at 4°C and then with the corresponding fluorescent secondary antibodies (dilution ratio: 1:800) at room temperature for 1 h. The whole process was done in a dark room and away from light. An appropriate amount of 4',6-diamidino-2-phenylindole (DAPI) dye solution was added for 30 min. The cells were then observed and photographed under a confocal microscope.

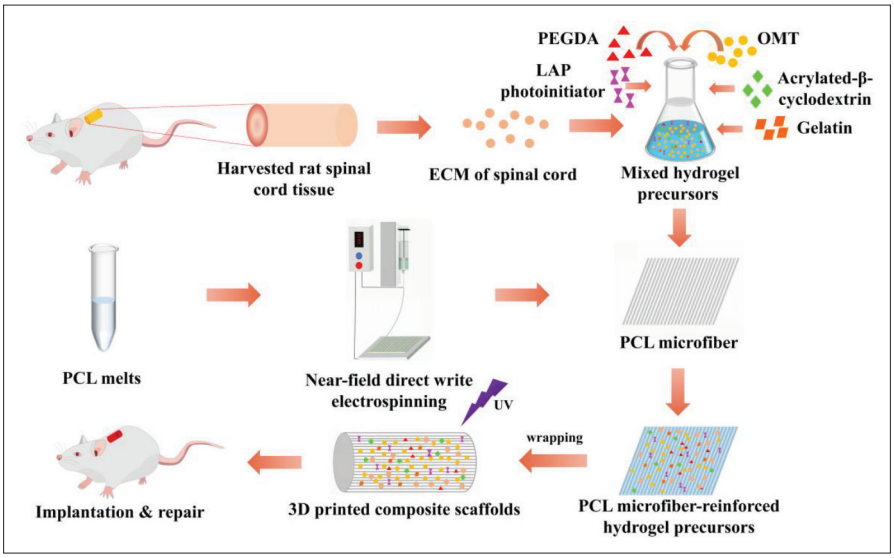

Figure 1. Fabrication by 3D bioprinting and implantation of spinal cord extracellular matrix (ECM) hydrogel microfiber scaffolds equipped with oxymatrine (OMT).

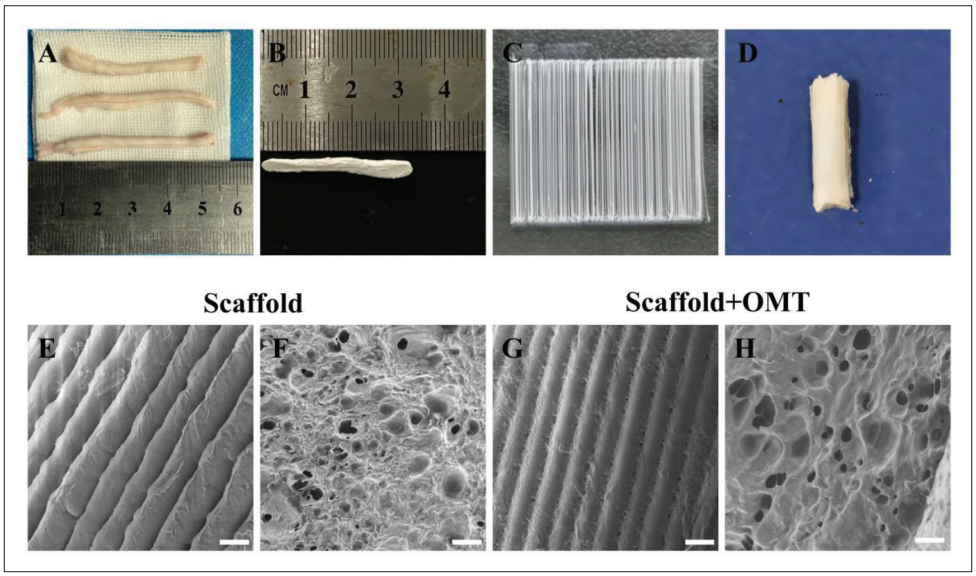

Figure 2. Characterization of scaffolds. (A) Normal spinal cord tissue. (B) Spinal cord decellularized scaffold. (C) PCL microfiber structure. (D) General morphology of the 3D-bioprinted composite scaffold. (E–H) Microstructure of scaffolds scanned by SEM. The images of scaffold and scaffold + OMT show parallel microfibers of the same thickness and hydrogels attached to the fibers. The inside of the scaffold showed uniform and dense pores, which could facilitate the growth of NSCs and the exchange of nutrients. Scale: 100 μm.

2.7. Establishment of a rat spinal cord hemitransection injury model and implantation of scaffolds

The rats were randomly divided into four groups: (i) sham group (only laminectomy without spinal cord injury, n = 10), (ii) SCI group (simple injury group without stent transplantation, n = 10), (iii) scaffold group (implantation of a scaffold after spinal cord injury, n = 10), and (iv) scaffold + OMT group (scaffold + OMT implanted after spinal cord injury, n = 10).

Under sterile conditions, the composite scaffold was pruned into cylindrical segments with a length of 2 mm for *in vivo* implantation. The specific surgical steps were as follows (as shown in Figure 2): 40 female SD rats were fed adaptively for 1 week. The night before the surgery, the rats were fasted but had access to water. All rats were anesthetized by 3% sodium pentobarbital (1 mL/kg) via intraperitoneal injection. The fur on the back was cleaned with 75% medical alcohol. The back of the rats was then shaved to expose their skin. The rats were placed in a prone

position on the animal operating table, and the limbs and heads were fixed. A towel with routine disinfection (iodine) was spread over the surgical site at the T10 level. The skin along the posterior midline was cut, and the musculature and soft tissues were bluntly dissected layer by layer to expose the vertebral body. A laminectomy was performed at T8–T12 using a rongeur (corneoscleral forceps). This was done under a microscope and under sterile conditions. A cut was made 2 mm left of the spinal cord segment at the level of T10 to form a 2.0-mm gap on the T10 spinal cord. A small suction device was used to aspirate the transected spinal cord tissue. The rat's left hind limb twitched, the left foot was dorsiflexed, and the muscles were relaxed and weak, indicating that the modeling was successful. The surgical port was flushed with 0.9% physiological sodium chloride. Following sufficient hemostasis after spinal cord injury, the corresponding scaffolds of each group were immediately transplanted to the defect site. The wound was sutured layer by layer and sterilized again with iodophor. Rats were resuscitated on an electric blanket and given a dose of penicillin to prevent infection.

2.8. Postoperative care and infection prevention

After the surgery, the rats were marked and kept in separate cages according to their group. Attention was given to the general condition and activities of the rats after the surgery. The rats were manually assisted daily with passive activities of both lower limbs. This was to avoid joint stiffness and muscle atrophy of the lower limbs so as not to affect the assessment of motor function. The rats' bladders were manually massaged daily for 2 weeks to assist in urination and reduce complications, such as urinary tract infection. Intramuscular injection of penicillin was given once a day for 1 week after surgery. Then, antibiotics or physiological sodium chloride solution were appropriately injected according to the rats' urine color, health status, and mental state. The litter was cleaned up frequently to keep the cage dry.

2.9. Assessment of motor function

Basso–Beattie–Bresnahan's (BBB) score was used to evaluate the recovery of hind limb motor function in rats after SCI. Scores were performed weekly for 1–8 weeks after surgery. A score of 0 means complete loss of motor function of the hind limbs, and a score of 21 means that the motor function of the hind limbs was normal. The behavioral assessment was independently completed by two experimenters who did not know the grouping. To avoid the impact of bladder filling on exercise, the rats were massaged for urination before the measurement.

2.10. Heart perfusion, sampling, and sectioning

Eight weeks after the surgery, the experimental rats were anesthetized by 3% sodium pentobarbital (1 mL/kg) via intraperitoneal injection and fixed in the supine position on the animal operating table. Routine disinfection and draping of towels were performed. After the onset of anesthesia, the skin of the rat chest was incised with a scalpel, and the subcutaneous tissue was bluntly stripped to expose the sternum and left rib. The pericardium was opened. An indwelling needle with suitable size was used to pierce the left ventricle at the apex of the heart, and the assistant helped to fix the needle to prevent it from withdrawing. An incision of about 5 mm was made in the right atrial appendage with ophthalmic scissors. First, a 250-mL syringe was used to extract physiological sodium chloride through the left ventricle. Perfusion was continued until the fluid flowing from the right atrial appendage became clear and transparent. At the same time, the rat's lung tissue and liver became pale and highly swollen. At this time, a 4% paraformaldehyde solution was used for continuous perfusion (whole-body muscle tremors were seen during the process, indicating the perfusion effect was good). After the perfusion was complete, the spinal cord tissue was removed and placed in a 4% paraformaldehyde solution. It was soaked in the test tube overnight. The next day, it was removed for gradient dehydration treatment with 15% and 30% sucrose solution or stored in a −80°C freezer. Finally, the embedded tissue blocks were placed in a cryostat for sectioning. The thickness of the slices was 6–15 μm. The sections could be directly stained or stored in a −80°C freezer.

2.11. Hematoxylin–eosin (H&E) staining

Selected sections were rinsed three times with PBS for 5 min each, hematoxylin staining solution for 5 min, tap water for 2 min, hydrochloric acid alcohol differentiation solution for 3 s, tap water for 2 min, and ammonia water for 3 s to blue. Sections were stained with eosin staining solution for 2 min and rinsed with tap water for 2 min. The sections were sequentially placed in 80% ethanol, 90% ethanol, and 100% ethanol twice for 1 min each time and put in xylene two times for 5 min each time. The sections were then placed in a fume hood to dry. After sealing with neutral gum, they were observed under a microscope.

2.12. Nissl staining

The washed sections were immersed in Nissl staining solution in a staining box, which was placed in a 37°C incubator, for 7 min. The sections were rinsed two times with PBS for 30 s each time, and placed in 95% ethanol for 30 s and in xylene solution two times for 5 min each time. Then, the sections were placed in a fume hood to dry. After sealing with neutral gum, the sections were observed under a microscope.

2.13. Immunofluorescence staining

The sections were selected and rinsed three times with PBS for 5 min each time. The washed sections were placed in

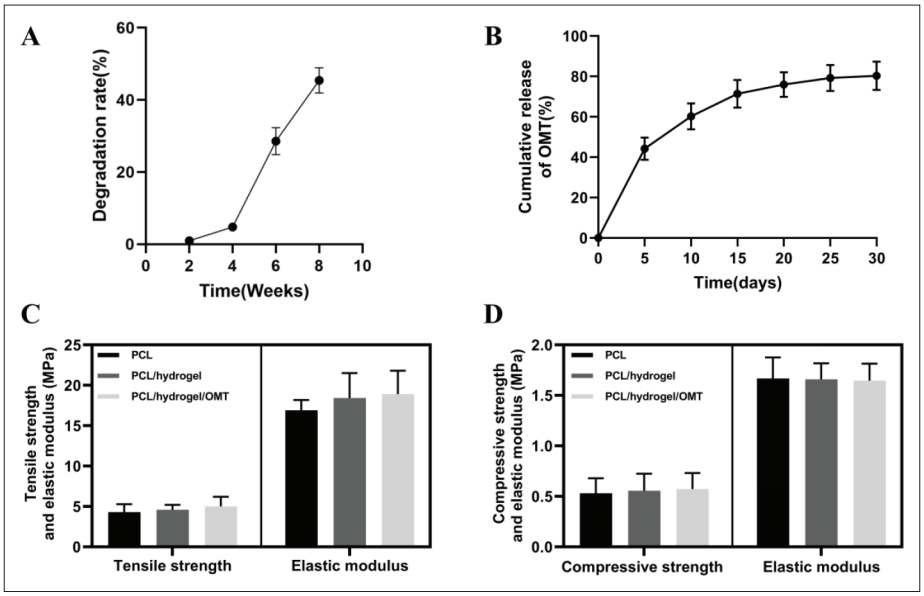

Figure 3. Characterization of scaffolds. (A) *In vitro* scaffold degradation curve. (B) Cumulative release curve of OMT *in vitro*. (C) The tensile strength and elastic modulus of the scaffold. (D) The compressive strength and elastic modulus of the scaffold.

TE9.0 antigen retrieval solution in a 60°C water bath for 4 h. The sections were taken out, cooled at room temperature for 15–30 min, and rinsed three times with PBS for 5 min each time. The sections were placed in a humidor, and 10% goat serum was added dropwise for blocking at room temperature for 1 h. Primary antibodies (nestin, TUJ1, MAP2, GFAP) were added and incubated with the sections in a humidor at 4°C overnight. The sections were rinsed three times with PBS for 5 min. A fluorescent secondary antibody (operated in a dark room) was added, and the sections were incubated at room temperature for 1 h in the dark. The sections were rinsed three times with PBS for 5 min (operating in a dark room). After the sections had dried, DAPI mounting medium was added dropwise. A coverglass was placed, and then the upper and lower ends of the coverglass were fixed with colorless nail polish. The sections were observed and photographed using a laser confocal microscope.

2.14. Statistical analysis

All experimental data were processed and plotted using GraphPad Prism 8.0. The data are expressed as the mean ± standard deviation (SD). ANOVA was used to test whether the obtained data had a statistical difference, and $p < 0.05$ indicated a statistical difference between the data.

3. Results

3.1. Characterization of scaffolds

Microfiber bundle-reinforced spinal cord ECM hydrogel scaffolds loaded with OMT were fabricated by near-field direct write electrospinning of aligned PCL microfiber bundles, coating of the spinal cord ECM hydrogel precursor on the PCL microfiber bundles, wrapping of the microfiber bundles/hydrogel layer into a cylindrical shape, and crosslinking with UV (Figure 2). Figure 2C shows the fibrous PCL bundles printed by near-field direct write electrospinning. It can be seen that the PCL microfibers were arranged in a linear and parallel manner. Figure 3D shows the macroscopic morphology of the composite hydrogel scaffold, which had a cylindrical shape. The microstructure of the scaffold was observed by SEM (Figure 2E–H). The composite scaffold had a biphasic structure in which a cylindrical spinal cord ECM hydrogel was penetrated longitudinally by the aligned microfiber bundle (Figure 2G). The freeze-dried spinal cord ECM hydrogel of the composite scaffold exhibited a porous honeycomb-like structure in which numerous internal pores were evenly distributed.

The *in vitro* degradation of the composite scaffolds was investigated (Figure 3A). The weight loss of the composite scaffolds gradually increased with increasing incubation time. No obvious degradation was observed in the initial 2 weeks. The degradation rate increased slowly in weeks 2–4, while the degradation rate increased rapidly in weeks 4–8. This demonstrated an accelerated scaffold degradation behavior. It is worth noting that the scaffold was not completely degraded at 8 weeks; the remaining weight was about 50%. This indicated that the scaffold's stability was sufficient to provide support for long-term nerve tissue regeneration.

Figure 3B shows the cumulative release curve of OMT. OMT can be released continuously from the scaffold, with

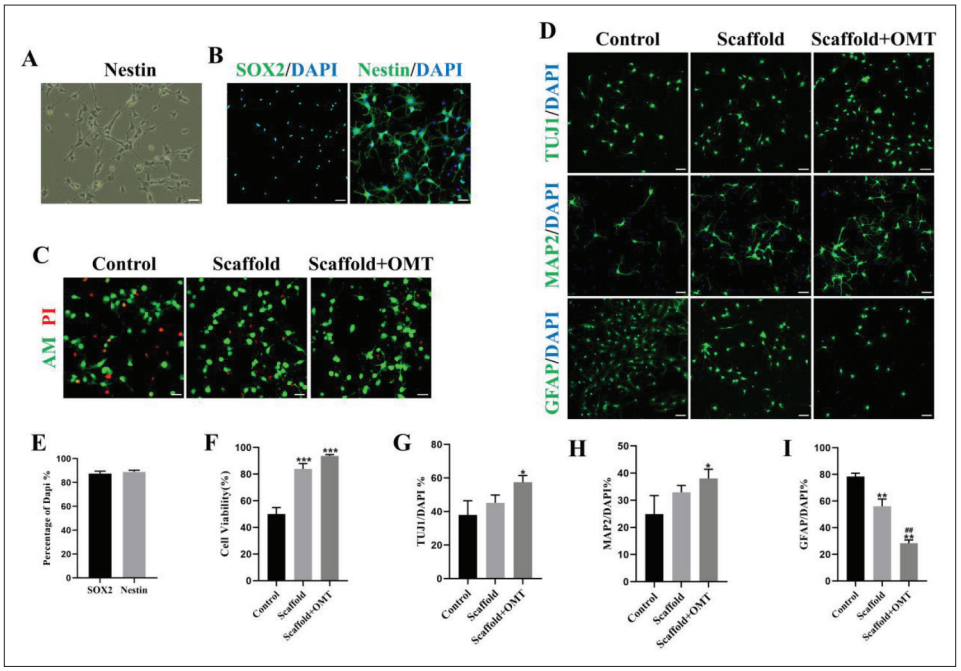

Figure 4. Biocompatibility of composite scaffolds. (A) Representative image of NSC morphology under a light microscope. (B) Nestin and SOX2 immunofluorescence-labeled NSCs. (C) Dead and alive assay of co-cultured NSCs with scaffolds; green represents live cells, and red represents dead cells. (D) Representative images of immunofluorescence staining of TUJ1, MAP2, and GFAP after NSCs were co-cultured with scaffolds for 7 days. (E) Quantitative analysis of nestin and SOX2 immunofluorescence staining. (F) Survival analysis of NSCs. (G) Semi-quantitative analysis of TUJ1 immunofluorescence staining. (H) Semi-quantitative analysis of MAP2 immunofluorescence staining. (I) Semi-quantitative analysis of GFAP immunofluorescence staining. All data are presented as the mean ± SD; n = 3 independent experiments. $^{*}p < 0.05$, $^{**}p < 0.01$, $^{***}p < 0.001$ vs. the control group. $^{\#\#}p < 0.01$ vs. the scaffold group. Scale bars = 50 μm (B–D).

rapid release in the first 2 weeks and slow release after 2 weeks. The cumulative release of OMT at 30 days was 80.32 ± 7.1%, indicating that OMT can achieve sustained release *in vitro*.

Figure 3C and D show the PCL scaffold, PCL/hydrogel scaffold, and PCL/hydrogel/OMT scaffold with similar tensile strengths (4.29 ± 0.98, 4.59 ± 0.60 mm, 5.00 ± 1.19 MPa) and elastic moduli (16.92 ± 1.27, 18.43 ± 3.09, 18.91 ± 2.90 MPa) ($p > 0.05$), compressive strengths (0.53 ± 0.15, 0.55 ± 0.14, 0.57 ± 0.13 MPa), and elastic moduli (1.67 ± 0.21, 1.66 ± 0.16, 1.69 ± 0.17 MPa) ($p > 0.05$), indicating that the composite scaffold had superior tension and compressive capacity, and could provide favorable living conditions for nerve regeneration.

3.2. *In vitro* biological performance of the composite scaffolds

The NSCs were co-cultured with the scaffolds, and the effect of the scaffolds on the viability and growth state of the NSCs was determined by the live and dead assay. Compared to the control group, the survival rates of NSCs in the scaffold group (83.96 ± 3.99%) and the scaffold + OMT group (93.71 ± 1.04%) were significantly higher (Figure 4C and F), suggesting that the composite scaffold and drug-loaded composite scaffold had sufficient biocompatibility for NSC growth.

NSCs co-cultured with scaffolds were subjected to immunofluorescence staining for TUJ1, MAP2, and GFAP to study the effect of drug-loaded scaffolds on *in vitro* NSC differentiation (Figure 4D and Figure S1). The results showed that both a drug-free scaffold and OMT-loaded scaffold could promote the differentiation of NSCs into neurons, as indicated by more $TUJ1^{+}$ and $MAP2^{+}$ cells. The effect on the neuronal differentiation of NSCs was more evident in the scaffold + OMT group than in the scaffold group ($p < 0.05$). On the contrary, differentiation of NSCs into astrocytes was significantly reduced in the scaffold + OMT group ($p < 0.05$).

3.3. Composite scaffolds loaded with OMT promoted motor function recovery

Eight weeks after surgery, cardiac perfusion samples were obtained. The gross observation showed that the texture of the lesion region filled either with the scaffold alone or OMT-loaded scaffold was similar to that of the uninjured spinal cord tissue. The scaffolds with or without OMT were well fused with the host spinal cord tissue. In the SCI group, defects/cavities could still be found

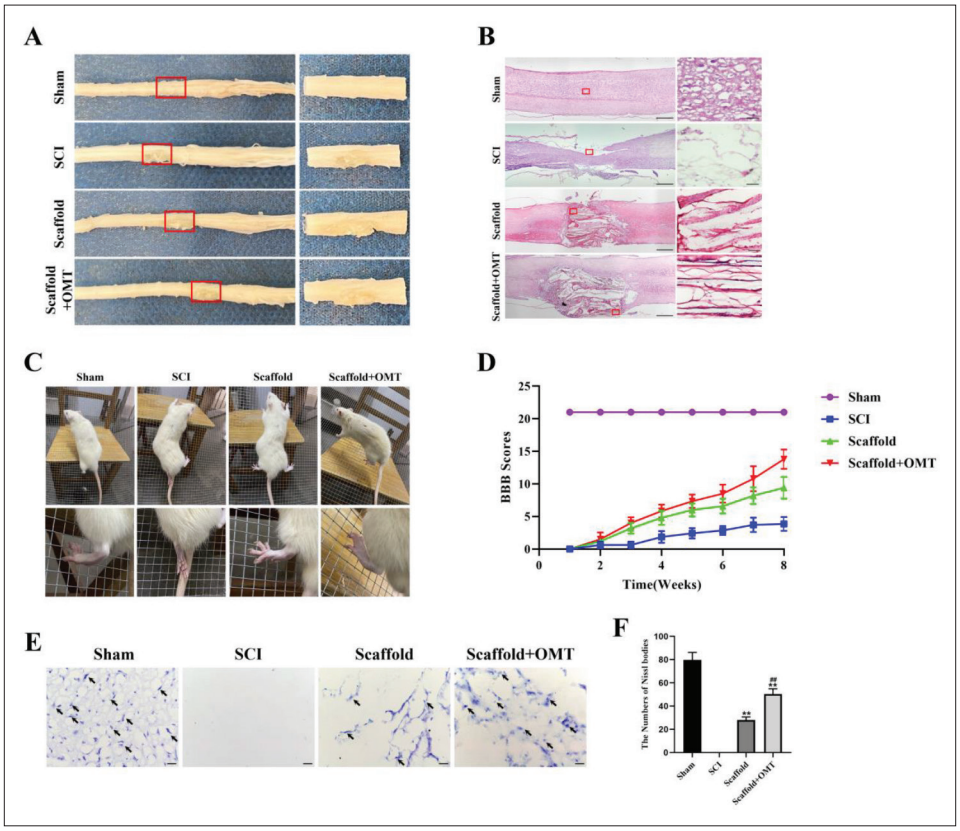

Figure 5. Assessment of histology and motor function. (A) Rat spinal cord tissue was obtained 8 weeks after the surgery, and the red box is the lesion site. (B) H&E-stained image of spinal cord longitudinal section. (C) Representative images of hind limb motor function recovery of rats in each group after the surgery. (D) Results of the BBB score of rats in each group from 1 to 8 weeks after surgery. (E) Representative images of Nissl staining results in each group 8 weeks after surgery. (F) Quantitative analysis of Nissl staining. n = 3, $^{**}p < 0.01$ vs. the control group. $^{\#\#}p < 0.01$ vs. the scaffold group. Scale bar = 1 mm (B) and 50 μm (B, E).

in the lesions, and severe scarring was also observed (Figure 5A). After SCI, the rats lost motor function in the left hind limb. Rats were assessed weekly after surgery for 8 weeks through BBB scores (Figure 5D). One to 2 weeks following surgery, the motor function in the hind limbs of rats in each group had not recovered significantly, and there was no significant difference in BBB scores among the different groups. However, at 3–8 weeks after the surgery, the scaffold-implanted rats showed sustained motor function recovery.

Longitudinal slices of the injured spinal cord were sectioned for H&E staining analysis (Figure 5B). Compared with the sham group, the SCI group exhibited a large number of visible voids with varied sizes and structures. In the scaffold group and scaffold + OMT group, the lesion site was compact and dense, and cells that had migrated from the host tissue could be observed. The Nissl staining results showed that there were no new neurons or Nissl corpuscles but many large cavities in the lesions in the SCI group. New neurons and Nissl bodies (in blue-purple color) were observed in the two groups with scaffolds with/without OMT. The scaffold + OMT group induced a significantly higher density of Nissl bodies than the other two groups (Figure 5E and F).

3.4. Composite scaffolds loaded with OMT promoted spinal cord tissue regeneration

Nestin, TUJ1, and MAP2 immunofluorescence staining was conducted to detect the regeneration of new neurons at the lesion site (Figure 6). The results showed that in the scaffold group and scaffold + OMT group, a small amount of nestin$^+$ cells and TUJ1$^+$ nerve tissue was found in the lesion site. However, no apparent newly regenerated nerve tissue was found in the lesions in the SCI group, suggesting that without the guidance of biological scaffolds after SCI, it was difficult for NSCs to migrate into the lesion site and establish new nerve conduction. We also found that TUJ1$^+$ neural tissue at the lesion site was longitudinally aligned in both groups with implanted composite scaffolds. This indicated that the parallel-arranged microfiber structures of the microfiber-reinforced spinal cord ECM hydrogel scaffolds could provide topographical guidance for neurite outgrowth to achieve more efficient nerve

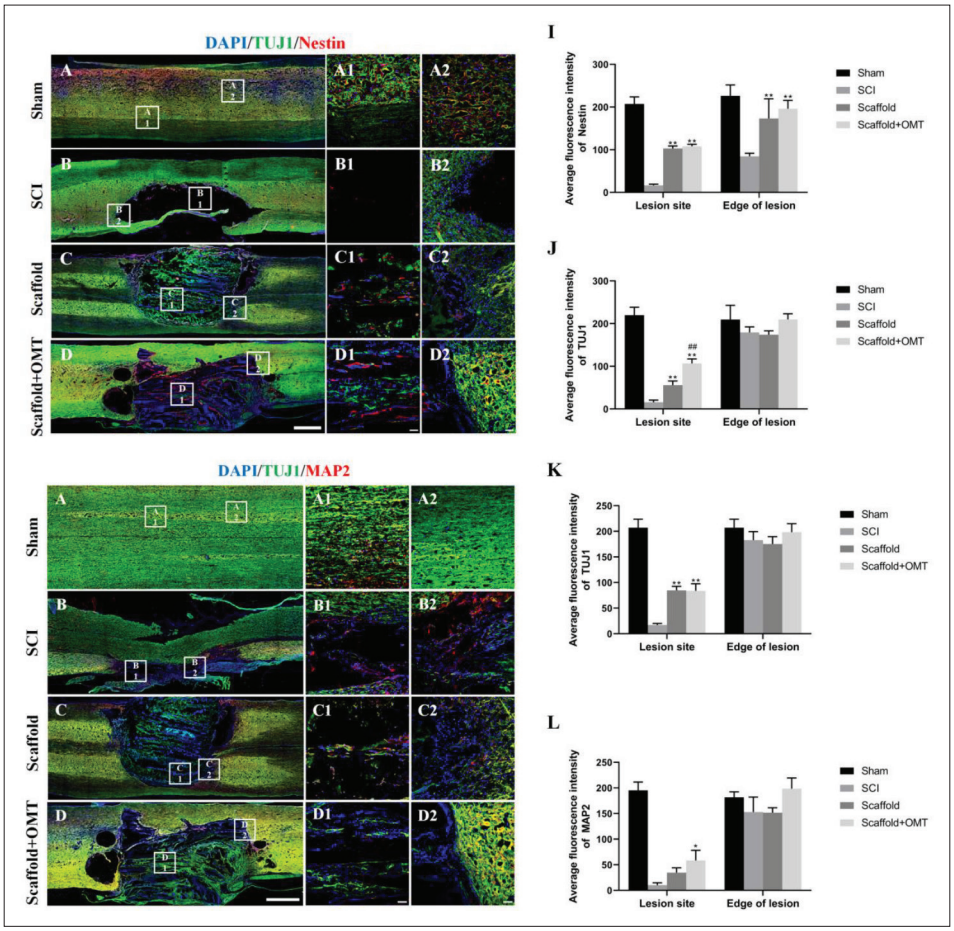

Figure 6. Composite scaffolds promote axon regeneration. (A–H) Representative images of immunofluorescence in each group 8 weeks after surgery. (A–A2, E–E2) Normal spinal cord tissue in the sham group. (B–D, B1–D1) Both the scaffold group and scaffold + OMT group had NSC migration and new axon ingrowth in the spinal cord lesions, but there was almost no nerve regeneration in the SCI group. (F–H, F1–H1) New axons growing into the scaffold along the spinal cord lesions were also seen, and there were a few MAP2-positive cells. (I) Nestin immunofluorescence semi-quantitative analysis. (J and K) Immunofluorescence semi-quantitative analysis of TUJ1. (L) MAP2 immunofluorescence semi-quantitative analysis. n = 3, $^{*}p < 0.05$ vs. the control group, $^{**}p < 0.01$ vs. the control group, $^{\#\#}p < 0.01$ vs. the scaffold group. Scale bars = 1 mm (A–H) and 50 μm (A1–H1, A2–H2).

regeneration. In addition, although TUJ1^{+} neurons were detected in the spinal cord lesions of the scaffold groups with/without OMT, the number of TUJ1^{+} neurons in the scaffold + OMT group was significantly higher than in the scaffold group ($p < 0.05$). Furthermore, the number of TUJ1^{+} neurons in the scaffold and scaffold + OMT groups were considerably higher than in the SCI group ($p < 0.01$). However, there was no statistical significance in nestin^{+} cells between the two groups. The above results suggested that implanting composite scaffolds with aligned features after SCI could promote the generation of new neurons in the injury site. The sustained release of OMT from drug-loaded composite scaffolds could further enhance neuron regeneration. This might be attributed to the fact that OMT could drive more endogenous NSCs to migrate to the center of the lesion along the PCL microfiber track and differentiate into neurons.

3.5. Composite scaffolds loaded with OMT alleviated glial scarring

Immunofluorescence staining for GFAP and MAP2 in the lesion areas showed that the composite scaffold had an inhibitory effect on GFAP expression (Figure 7). Fewer GFAP^{+} cells and many MAP2^{+} cells were observed in the sham group. The lesion in the SCI group presented a large cavity, and almost no cells could be observed (Figure 7B). In contrast, a large number of astrocytes had proliferated and were activated around the lesion (Figure 7B2). In the scaffold group, more GFAP^{+} cells were observed in the transplanted area, and many astrocytes had proliferated and were activated around the lesion (Figure 7C2). In comparison, only a few GFAP^{+} cells were observed in and around the lesion in the scaffold + OMT group, showing a relatively sparse distribution of GFAP^{+} cells. However, only a few MAP2^{+} cells were found in the scaffold region of the

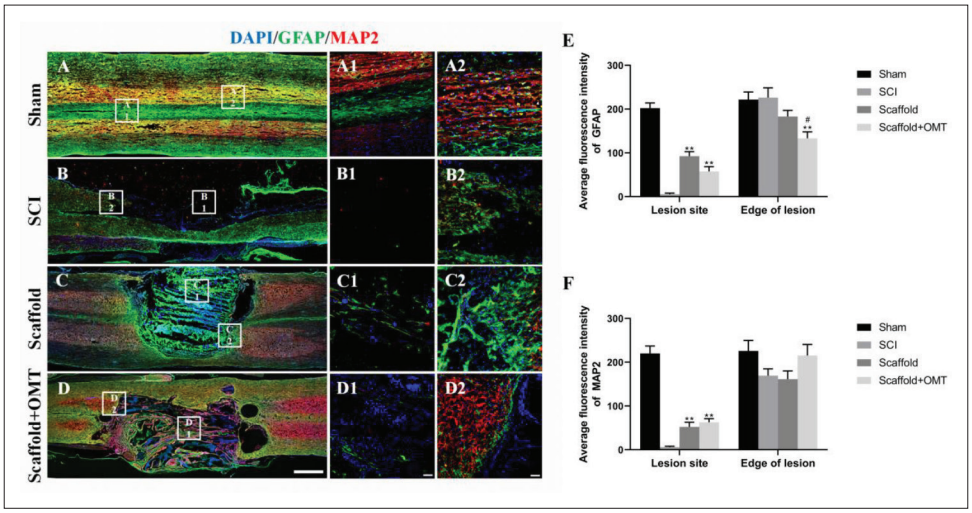

Figure 7. The composite scaffold alleviates the formation of glial scars. (A–D) Representative images of immunofluorescence in each group 8 weeks after surgery. (A–A2) Normal spinal cord tissue in the sham group. (B–D, B1–D1) Compared with the SCI group, a small number of astrocytes were expressed in the spinal cord lesions of the scaffold group and the scaffold + OMT group. (B2–D2) Compared with the SCI group, the expression of GFAP-positive cells around the spinal cord lesions in the scaffold group and the scaffold + OMT group was significantly decreased; the scaffold + OMT group was more significant. (E) GFAP immunofluorescence semi-quantitative analysis. (F) MAP2 immunofluorescence semi-quantitative analysis. n = 3, $^{**}p < 0.01$ vs. the control group, $^{\#}p < 0.05$ vs. the scaffold group. Scale bars = 1 mm (A–D) and 50 μm (A1–D1, A2–D2).

scaffold group and scaffold + OMT group, suggesting that the presence of OMT effectively inhibited the proliferation and activation of astrocytes, hence reducing the formation of glial scars and eliminating obstacles to neurite extension.

4. Discussion

The treatment of SCI remains a significant challenge. As the self-regeneration capacity of the human central nervous system is weak[38], several strategies have been developed, including cell implantation, hydrogel injection, drug therapy, and scaffold implantation. However, effective interventions for acute and chronic SCI are still limited, despite achievements in both basic and clinical research[38,39].

Tissue engineering scaffolds have always been a research hotspot in the field of tissue engineering. Numerous studies have demonstrated the advantages of scaffolds in delivering cells and drugs to repair or regenerate the central nervous system[38]. However, in previous studies, scaffolds were mainly in the form of fibrous/porous scaffolds or hydrogel scaffolds[40-42]. In this study, near-field direct write electrospinning was used to fabricate PCL microfiber bundles, which act as the backbone of the composite scaffold, while the spinal cord ECM-based OMT-containing hydrogel was used as the hydrogel matrix of the composite scaffolds. PCL, a synthetic biodegradable polyester, has been fabricated into various biological scaffolds for nerve regeneration and SCI research[43-45]. Spinal cord ECM is a natural material, and it possesses the advantages of a natural 3D structure, excellent biocompatibility, and very low immunogenicity[46]. Studies have found that spinal cord ECM-based hydrogels can regulate the behavior of NSCs and promote their differentiation toward a neuronal lineage[31,47]. Our results showed that the composite scaffolds had excellent biocompatibility, degradability, and mechanical property. They could provide a stable and suitable microenvironment for nerve regeneration and guide new axons to grow into the lesion site. These axons grew along with the longitudinal direction of the PCL microfiber bundles. Zhang *et al.* also used electrospinning technology to prepare PCL/polysialic acid hybrid multifunctional nanofiber scaffolds, and the scaffolds could promote axonal growth and functional recovery after SCI in rats[48]. Wang *et al.* constructed a cytokine-loaded PCL–PEG composite hydrogel scaffold, which could also guide the directional growth of axons[49]. In addition, Xing *et al.* constructed an acellular spinal cord scaffold cross-linked NT-3 sustained-release system, which promoted adhesion, proliferation, and differentiation of rat bone marrow mesenchymal stem cells[50]. The slow degradation of PCL can provide sufficient time for nerve regeneration for the growth of new axons at both ends and the establishment of new connections.

After SCI, axon regeneration is usually promoted by implanting exogenous NSCs or activating endogenous NSCs. Because NSCs have multi-directional differentiation potential, it is crucial to induce their differentiation toward neurons. Some studies stimulated the activation and migration of endogenous NSCs by administering some small biological/chemical molecules that promoted axon regeneration[51,52]. In our study, the immunofluorescence

staining results of the nestin$^+$ cells in and around the lesions in the scaffold group and scaffold + OMT group indicated that some components of the composite scaffold might positively affect the activation and migration of endogenous NSCs. In addition, composite scaffolds could induce the differentiation of NSCs toward neurons and promote their maturation. OMT has anti-inflammatory, antioxidant, and anti-fibrosis effects. After the occurrence of SCI, inflammatory mediators and oxidizing substances will be produced at the injured site. The addition of OMT may inhibit further development of inflammation at the injured site, and reportedly, OMT can promote the repair of SCI. Thus, the addition of OMT may promote nerve regeneration.

After SCI, astrocytes at the lesion site and around the lesion usually proliferate and activate in large quantities to form glial scars[53], which are undoubtedly a significant obstacle to the regeneration of the central nervous system. Most of the previous studies were focused on effectively promoting nerve regeneration, whereas only a few studies were focused on preventing glial scarring[54,55]. OMT is a Chinese patented medicine that inhibits the fibrosis of various tissues and organs[35,56]. Relevant studies have shown that intraperitoneal injection of different doses of OMT could promote recovery from SCI to different degrees, but its effect on glial scars is unknown[36]. Therefore, we encapsulated OMT into composite scaffolds to explore whether it could inhibit glial scarring. The results confirmed that the scaffold + OMT group had the least number of GFAP$^+$ cells, indicating that OMT plays a role in inhibiting glial scarring. Unlike previous studies that directly injected OMT into the lesion site to achieve only a short-term drug delivery, we loaded OMT into the hydrogel, which avoided its rapid removal from the body and achieved a sustained release.

Activation of microglia and production of various cytokines after SCI leads to increased inflammatory response and enhanced activation of TGF-β and Smad2 pathways[57]. The GF-β/Smad pathway contributes to scar formation and plays a role in recovery from injury, but excessive scar tissue formation can interfere with functional recovery[58]. OMT can inhibit the TGF-β/Smad pathway[59,60]. Our study found an interesting phenomenon, that is, the release of OMT affects the differentiation direction of NSCs and can inhibit the expression of astrocytes, thus reducing the formation of the glial scar. We speculated that it may be related to the TGF-β/Smad signaling pathway, which will be further studied in the future.

One drawback of this study is that it is difficult to obtain an ECM of the human spinal cord. Therefore, we resorted to using ECM of the spinal cord in rats, which is relatively easy to obtain. In the future, we will continue to conduct in-depth research and try to explore other tissues or organs that can replace the ECM of the spinal cord.

5. Conclusion

In this study, we fabricated PCL microfiber-reinforced spinal cord ECM hydrogel-based scaffolds loaded with OMT. The composite scaffolds promoted the differentiation of NSCs into neurons and inhibited the differentiation of NSCs into astrocytes. Composite scaffolds provided a suitable microenvironment for *in vivo* spinal cord tissue regeneration and guided the directional growth of axons. OMT further promoted nerve regeneration and reduced the formation of glial scaring around the lesions. In addition, the transplantation of a scaffold with OMT significantly improved the motor function of rats with SCI. This study suggests a simple way to fabricate advanced materials with the required composition, desirable topographical cues, and excellent therapeutic capability for the clinical treatment of SCI.

Acknowledgments

None.

Funding

This work was supported by National Natural Science Foundation of China (Grant No. 32160209, 82160357 and 82071361), and Guangxi Key Laboratory of Basic and Translational Research of Bone and Joint Degenerative Diseases, China (Grant No. 21-220-06). Department of Education of Guangdong Province, China (2021ZDZX2014), Key Science and Technology Project of Social Development Foundation of Dongguan, China (20211800904542).

Conflict of interest

The authors have no conflicts of interest to declare.

Author contributions

Conceptualization: Yujin Tang, Jia Liu
Formal analysis: Jing Zhou, Junming Wan, Xingchang Zhao, Liqiang Wang
Investigation: Shiqiang Song, Xingchang Zhao
Methodology: Chengliang Yang, Chuanchuan Zheng
Supervision: Yujin Tang, Jia Liu
Writing – original draft: Shiqiang Song
Writing – review & editing: Chong Wang, Kai Li

Ethics approval and consent to participate

The animal experiments in this study were approved and agreed by the Animal Ethics Committee of Youjiang Medical University for Nationalities.

Consent for publication

Not applicable.

Availability of data

The data that support the findings of this study are available from the corresponding author upon reasonable request.

References

1. Wyndaele M, 2006, Incidence, prevalence and epidemiology of spinal cord injury: What learns a worldwide literature survey? *Spinal Cord*, 44(9):523–529.

   https://doi.org/10.1038/sj.sc.3101893

2. Scivoletto G, Miscusi M, Forcato S, *et al.*, 2017, The rehabilitation of spinal cord injury patients in Europe. *Acta Neurochir Suppl*, 124:203–210.

   https://doi.org/10.1007/978-3-319-39546-3_31

3. Rupp R, 2020, Spinal cord lesions. *Handb Clin Neurol*, 168:51–65.

   https://doi.org/10.1016/B978-0-444-63934-9.00006-8

4. Guo S, 2021, Spinal cord repair: From cells and tissue engineering to extracellular vesicles. *Cells*, 10(8):1872.

   https://doi.org/10.3390/cells10081872

5. Shi Z, Yuan S, Shi L, *et al.*, 2021, Programmed cell death in spinal cord injury pathogenesis and therapy. *Cell Prolif*, 54(3):e12992.

   https://doi.org/10.1111/cpr.12992

6. Chen X, Wang Y, Zhou G, *et al.*, 2021, The combination of nanoscaffolds and stem cell transplantation: Paving a promising road for spinal cord injury regeneration. *Biomed Pharmacother*, 143:112233.

   https://doi.org/10.1016/j.biopha.2021.112233

7. Zawadzka M, Kwasniewska A, Miazga K, *et al.*, 2021, Perspectives in the cell-based therapies of various aspects of the spinal cord injury-associated pathologies: Lessons from the animal models. *Cells*, 10(11):2995.

   https://doi.org/10.3390/cells10112995

8. Xiao Z, Tang F, Zhao Y, *et al.*, 2018, Significant improvement of acute complete spinal cord injury patients diagnosed by a combined criteria implanted with neuroregen scaffolds and mesenchymal stem cells. *Cell Transplant*, 27(6): 907–915.

   https://doi.org/10.1177/0963689718766279

9. Zhang Y, Al MA, Yuan Y, *et al.*, 2021, Acute spinal cord injury: Pathophysiology and pharmacological intervention (Review). *Mol Med Rep*, 23(6):417.

   https://doi.org/10.3892/mmr.2021.12056

10. Gedde MH, Lilleberg HS, Assmus J, *et al.*, 2019, Traumatic vs non-traumatic spinal cord injury: A comparison of primary rehabilitation outcomes and complications during hospitalization. *J Spinal Cord Med*, 42(6):695–701.

    https://doi.org/10.1080/10790268.2019.1598698

11. Haddad AF, 2021, The natural history of spinal cord injury. *Neurosurg Clin N Am*, 32(3):315–321.

    https://doi.org/10.1016/j.nec.2021.03.003

12. Fan B, Wei Z, Yao X, *et al.*, 2018, Microenvironment imbalance of spinal cord injury. *Cell Transplant*, 27(6): 853–866.

    https://doi.org/10.1177/0963689718755778

13. Vijayavenkataraman S, Yan WC, Lu WF, *et al.*, 2018, 3D bioprinting of tissues and organs for regenerative medicine. *Adv Drug Deliv Rev*, 132:296–332.

    https://doi.org/10.1016/j.addr.2018.07.004

14. Luo Y, 2018, 3D bioprinting of artificial tissues: Construction of biomimetic microstructures. *Macromol Biosci*, 18(6):e1800034.

    https://doi.org/10.1002/mabi.201800034

15. Junka R, 2020, Acellular polycaprolactone scaffolds laden with fibroblast/endothelial cell-derived extracellular matrix for bone regeneration. *J Biomed Mater Res A*, 108(2): 351–364.

    https://doi.org/10.1002/jbm.a.36821

16. He J, Li Z, Yu T, et al., 2020, Preparation and evaluation of acellular sheep periostea for guided bone regeneration. *J Biomed Mater Res A*, 108(1):19–29.

    https://doi.org/10.1002/jbm.a.36787

17. Gong M, Sun J, Liu G, *et al.*, 2021, Graphene oxide-modified 3D acellular cartilage extracellular matrix scaffold for cartilage regeneration. *Mater Sci Eng C Mater Biol Appl*, 119:111603.

    https://doi.org/10.1016/j.msec.2020.111603

18. Zhao Y, Zhao X, Zhang R, *et al.*, 2020, Cartilage extracellular matrix scaffold with kartogenin-encapsulated PLGA microspheres for cartilage regeneration. *Front Bioeng Biotechnol*, 8:600103.

    https://doi.org/10.3389/fbioe.2020.600103

19. Urciuolo A, 2018, Decellularized tissue for muscle regeneration. *Int J Mol Sci*, 19(8):2392.

    https://doi.org/10.3390/ijms19082392

20. Dhasmana A, Singh L, Roy P, *et al.*, 2019, Silk fibroin protein modified acellular dermal matrix for tissue repairing and regeneration. *Mater Sci Eng C Mater Biol Appl*, 97:313–324.

    https://doi.org/10.1016/j.msec.2018.12.038

21. Perveen S, Rossin D, Vitale E, *et al.*, 2021, Therapeutic acellular scaffolds for limiting left ventricular remodelling-current status and future directions. *Int J Mol Sci*, 22(23):13054.

    https://doi.org/10.3390/ijms222313054

22. Eitan Y, Sarig U, Dahan N, *et al.*, 2010, Acellular cardiac extracellular matrix as a scaffold for tissue engineering: In vitro cell support, remodeling, and biocompatibility. *Tissue Eng Part C Methods*, 16(4):671–683.

    https://doi.org/10.1089/ten.TEC.2009.0111

23. Esmaeili PK, Mashayekhan S, Asl SG, *et al.*, 2018, Construction of scaffolds composed of acellular cardiac extracellular matrix for myocardial tissue engineering. *Biologicals*, 53:10–18.

    https://doi.org/10.1016/j.biologicals.2018.03.005

24. Ilanlou S, Khakbiz M, Amoabediny G, *et al.*, 2019, Preclinical studies of acellular extracellular matrices as small-caliber vascular grafts. *Tissue Cell*, 60:25–32.

    https://doi.org/10.1016/j.tice.2019.07.008

25. Horst M, Milleret V, Noetzli S, *et al.*, 2017, Polyesterurethane and acellular matrix based hybrid biomaterial for bladder engineering. *J Biomed Mater Res B Appl Biomater*, 105(3):658–667.

    https://doi.org/10.1002/jbm.b.33591

26. Guan Y, Liu S, Liu Y, *et al.*, 2015, Porcine kidneys as a source of ECM scaffold for kidney regeneration. *Mater Sci Eng C Mater Biol Appl*, 56:451–456.

    https://doi.org/10.1016/j.msec.2015.07.007

27. Huang D, 2016, Cogels of hyaluronic acid and acellular matrix for cultivation of adipose-derived stem cells: Potential application for vocal fold tissue engineering. *Biomed Res Int*, 2016:6584054.

    https://doi.org/10.1155/2016/6584054

28. Ge L, Arul K, Ikpeze T, *et al.*, 2018, Traumatic and nontraumatic spinal cord injuries. *World Neurosurg*, 111:e142–e148.

    https://doi.org/10.1016/j.wneu.2017.12.008

29. Miyazaki K, 2014, Partial regeneration and reconstruction of the rat uterus through recellularization of a decellularized uterine matrix. *Biomaterials*, 35(31):8791–8800.

    https://doi.org/10.1016/j.biomaterials.2014.06.052

30. Wang F, Maeda Y, Zachar V, *et al.*, 2018, Regeneration of the oesophageal muscle layer from oesophagus acellular matrix scaffold using adipose-derived stem cells. *Biochem Biophys Res Commun*, 503(1):271–277.

    https://doi.org/10.1016/j.bbrc.2018.06.014

31. Xu Y, Zhou J, Liu C, *et al.*, 2021, Understanding the role of tissue-specific decellularized spinal cord matrix hydrogel for neural stem/progenitor cell microenvironment reconstruction and spinal cord injury. *Biomaterials*, 268:120596.

    https://doi.org/10.1016/j.biomaterials.2020.120596

32. Haggerty AE, 2017, Extracellular matrix components as therapeutics for spinal cord injury. *Neurosci Lett*, 652:50–55.

    https://doi.org/10.1016/j.neulet.2016.09.053

33. Liu J, Chen J, Liu B, *et al.*, 2013, Acellular spinal cord scaffold seeded with mesenchymal stem cells promotes long-distance axon regeneration and functional recovery in spinal cord injured rats. *J Neurol Sci*, 325(1-2):127–136. The original reference was retracted by the journal office.

    https://doi.org/10.1016/j.jns.2012.11.022

34. Lan X, Zhao J, Zhang Y, *et al.*, 2020, Oxymatrine exerts organ- and tissue-protective effects by regulating inflammation, oxidative stress, apoptosis, and fibrosis: From bench to bedside. *Pharmacol Res*, 151:104541.

    https://doi.org/10.1016/j.phrs.2019.104541

35. Deng X, Zhao F, Zhao D, *et al.*, 2021, Oxymatrine promotes hypertrophic scar repair through reduced human scar fibroblast viability, collagen and induced apoptosis via autophagy inhibition. *Int Wound J*, 19(5):1221–1231.

    https://doi.org/10.1111/iwj.13717

36. Guan B, Chen R, Zhong M, *et al.*, 2020, Protective effect of oxymatrine against acute spinal cord injury in rats via modulating oxidative stress, inflammation and apoptosis. *Metab Brain Dis*, 35(1):149–157.

    https://doi.org/10.1007/s11011-019-00528-8

37. Tanabe N, Kuboyama T, Kazuma K, *et al.*, 2015, The extract of roots of *Sophora flavescens* enhances the recovery of motor function by axonal growth in mice with a spinal cord injury. *Front Pharmacol*, 6:326.

    https://doi.org/10.3389/fphar.2015.00326

38. Wang Q, Zhang H, Xu H, *et al.*, 2018, Novel multi-drug delivery hydrogel using scar-homing liposomes improves spinal cord injury repair. *Theranostics*, 8(16):4429–4446.

    https://doi.org/10.7150/thno.26717

39. Fuhrmann T, 2017, Combinatorial therapies after spinal cord injury: How can biomaterials help? *Adv Healthc Mater*, 6(10):1601130.

    https://doi.org/10.1002/adhm.201601130

40. Usmani S, Franceschi Biagioni A, Medelin M, *et al.*, 2020, Functional rewiring across spinal injuries via biomimetic nanofiber scaffolds. *Proc Natl Acad Sci*, 117(41):25212–25218.

    https://doi.org/10.1073/pnas.2005708117

41. Kourgiantaki A, Tzeranis DS, Karali K, *et al.*, 2020, Neural stem cell delivery via porous collagen scaffolds promotes

neuronal differentiation and locomotion recovery in spinal cord injury. *NPJ Regen Med*, 5(1):12.

https://doi.org/10.1038/s41536-020-0097-0

42. Sever Bahcekapili M, Yilmaz C, Demirel A, *et al.*, 2021, Neuroactive peptide nanofibers for regeneration of spinal cord after injury. *Macromol Biosci*, 21(1):2000234.

https://doi.org/10.1002/mabi.202000234

43. Sajadi E, Aliaghaei A, Farahni RM, *et al.*, 2021, Tissue plasminogen activator loaded PCL nanofibrous scaffold promoted nerve regeneration after sciatic nerve transection in male rats. *Neurotox Res*, 39(2):413–428.

https://doi.org/10.1007/s12640-020-00276-z

44. Babaloo H, Ebrahimi Barough S, Derakhshan MA, *et al.*, 2018, PCL/gelatin nanofibrous scaffolds with human endometrial stem cells/schwann cells facilitate axon regeneration in spinal cord injury. *J Cell Physiol*, 234(7):11060–11069.

https://doi.org/10.1002/jcp.27936

45. Rahimi-Sherbaf F, Nadri S, Rahmani A, *et al.*, 2020, Placenta mesenchymal stem cells differentiation toward neuronal-like cells on nanofibrous scaffold. *BioImpacts*, 10(2):117–122.

https://doi.org/10.34172/bi.2020.14

46. Tukmachev D, Forostyak S, Koci Z, *et al.*, 2016, Injectable extracellular matrix hydrogels as scaffolds for spinal cord injury repair. *Tissue Eng Part A*, 22(3-4):306–317.

https://doi.org/10.1089/ten.TEA.2015.0422

47. Ozudogru E, Isik M, Eylem CC, *et al.*, 2021, Decellularized spinal cord meninges extracellular matrix hydrogel that supports neurogenic differentiation and vascular structure formation. *J Tissue Eng Regen Med*, 15(11):948–963.

https://doi.org/10.1002/term.3240

48. Zhang S, Wang XJ, Li WS, *et al.*, 2018, Polycaprolactone/polysialic acid hybrid, multifunctional nanofiber scaffolds for treatment of spinal cord injury. *Acta Biomater*, 77:15–27.

https://doi.org/10.1016/j.actbio.2018.06.038

49. Wang P, Wang H, Ma K, *et al.*, 2020, Novel cytokine-loaded PCL-PEG scaffold composites for spinal cord injury repair. *RSC Adv*, 10(11):6306–6314.

https://doi.org/10.1039/c9ra10385f

50. Xing H, Ren X, Yin H, *et al.*, 2019, Construction of a NT-3 sustained-release system cross-linked with an acellular spinal cord scaffold and its effects on differentiation of cultured bone marrow mesenchymal stem cells. *Mater Sci Eng C*, 104:109902.

https://doi.org/10.1016/j.msec.2019.109902

51. Yang Y, Fan Y, Zhang H, *et al.*, 2021, Small molecules combined with collagen hydrogel direct neurogenesis and migration of neural stem cells after spinal cord injury. *Biomaterials*, 269:120479.

https://doi.org/10.1016/j.biomaterials.2020.120479

52. Li X, Fan C, Xiao Z, *et al.*, 2018, A collagen microchannel scaffold carrying paclitaxel-liposomes induces neuronal differentiation of neural stem cells through Wnt/beta-catenin signaling for spinal cord injury repair. *Biomaterials*, 183:114–127.

https://doi.org/10.1016/j.biomaterials.2018.08.037

53. Okada S, Hara M, Kobayakawa K, *et al.*, 2018, Astrocyte reactivity and astrogliosis after spinal cord injury. *Neurosci Res*, 126:39–43.

https://doi.org/10.1016/j.neures.2017.10.004

54. Bai Y, Lai B, Han W, *et al.*, 2021, Decellularized optic nerve functional scaffold transplant facilitates directional axon regeneration and remyelination in the injured white matter of the rat spinal cord. *Neural Regen Res*, 16(11):2276.

https://doi.org/10.4103/1673-5374.310696

55. Sadik ME, Ozturk AK, Albayar A, *et al.*, 2020, A strategy toward bridging a complete spinal cord lesion using stretch-grown axons. *Tissue Eng Part A*, 26(11-12):623–635.

https://doi.org/10.1089/ten.TEA.2019.0230

56. Lan X, Zhao J, Zhang Y, *et al.*, 2020, Oxymatrine exerts organ- and tissue-protective effects by regulating inflammation, oxidative stress, apoptosis, and fibrosis: From bench to bedside. *Pharmacol Res*, 151:104541.

https://doi.org/10.1016/j.phrs.2019.104541

57. Nathan FM, Li S, 2017, Environmental cues determine the fate of astrocytes after spinal cord injury. *Neural Regen Res*, 12(12):1964–1970.

https://doi.org/10.4103/1673-5374.221144

58. Gomes FC, Sousa VO, Romao L, 2005, Emerging roles for TGF-beta1 in nervous system development. *Int J Dev Neurosci*, 23(5):413–424.

https://doi.org/10.1016/j.ijdevneu.2005.04.001

59. Liu L, Lu W, Ma Z, *et al.*, 2012, Oxymatrine attenuates bleomycin-induced pulmonary fibrosis in mice via the inhibition of inducible nitric oxide synthase expression and the TGF-beta/Smad signaling pathway. *Int J Mol Med*, 29(5):815–822.

https://doi.org/10.3892/ijmm.2012.923

60. Zhao HW, Zhang ZF, Chai X, *et al.*, 2016, Oxymatrine attenuates CCl4-induced hepatic fibrosis via modulation of TLR4-dependent inflammatory and TGF-beta1 signaling pathways. *Int Immunopharmacol*, 36:249–255.

https://doi.org/10.1016/j.intimp.2016.04.040